ACS APPLIED MATERIALS & INTERFACES

Research Article

www.acsami.org

Preparation of a Stable Sol Suspension of Pd-Loaded SnO_2 Nanocrystals by a Photochemical Deposition Method for Highly Sensitive Semiconductor Gas Sensors

Masayoshi Yuasa,* Tetsuya Kida, and Kengo Shimanoe

Department of Energy and Material Sciences, Faculty of Engineering Sciences, Kyushu University, Kasuga-koen 6-1, Kasuga-shi, Fukuoka 816-8580, Japan

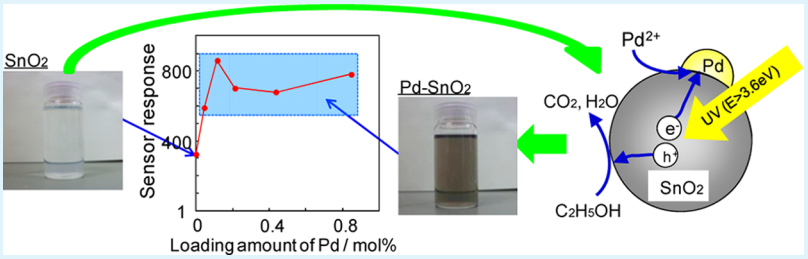

ABSTRACT: A stable sol suspension of Pd-loaded SnO_2 nanocrystals, which is valid for both fundamental studies of semiconductor gas sensor and fabrications of a micro gas sensor, was fabricated by the photochemical deposition of $PdCl_4^{2-}$ onto SnO_2 in an aqueous solution. UV light was irradiated on a mixture of a SnO_2 sol obtained through a hydrothermal treatment of stannic acid gel in the presence of $PdCl_4^{2-}$ and ethanol/water at pH 2. A stable sol suspension of Pd-loaded SnO_2 was successfully obtained by controlling the pH of the above suspension to 10.5 after UV irradiation. Thin-film type sensor devices (film thickness ~200 nm) using Pd-loaded SnO_2 nanocrystal were successfully fabricated by a spin-coating method. Gas sensing measurements showed that the deposition of Pd on the SnO_2 nanocrystals resulted in large electrical sensitization effect. The maximum gas sensitization effect was obtained at 0.125 mol % Pd loading. Moreover, the Pd loading lowered the temperature, in which the maximum sensor response to H_2 was obtained, due to the efficient catalytic combustion of H_2 on Pd.

KEYWORDS: *gas sensor, semiconductor, nanoparticle, receptor, photochemical deposition*

INTRODUCTION

The oxide semiconductor gas sensors have been practically used for detecting gases such as inflammable gases, hazardous gases, and environmental gases.[1] In particular, tin dioxide (SnO_2) has been extensively used as the gas sensing material due to some of its advantageous properties, such as high gas sensitivity, high stability, and low cost.[2,3] The gas sensing mechanism of oxide semiconductor gas sensors using SnO_2 has been considered that the target gases diffuse into the porous gas sensing films made from the SnO_2 particles and oxidized by the oxygen species absorbed on the SnO_2 surface, leading to the change in electric resistance.[4,5]

So far, extensive studies have revealed that the following three basic factors are important for improving the sensor response of oxide semiconductor sensor;[3] (1) transducer function of metal oxide crystal, (2) utility factor of gas sensing films (microstructure control of gas sensing films), and (3) receptor function (loading of receptors such as noble metals or metal oxides). As concerned with the transducer function, Xu et al. have reported that the sensor response increases drastically with decreasing the crystalline size of SnO_2 less than ~6 nm.[6] Moreover, recently, Yamazoe et al. have proposed the theoretical model and formula of the depletion state of semiconductor crystallite.[7−9] For the utility factor of the gas sensing film, the importance of the microstructure of the sensing film has been investigated experimentally and theoretically.[10−12] Baik et al. prepared a stable sol of SnO_2 nanocrystal by a hydrothermal treatment of a precipitated stannic acid gel in an ammonium solution and investigated the dependence of CO and H_2 response on the film thickness.[13,14] Sakai et al. controlled the microstructure of the SnO_2 thin film by adding the polyethylene glycol (PEG) to the sol of SnO_2 nanocrystal to be spin-coated. For the receptor function, it is well-known that loading of additives such as metals and metal oxides promotes the gas sensitivity or gas selectivity of the oxide semiconductor gas sensor.[15−20] In particular, Pd or PdO is frequently loaded on SnO_2 particles because of its electrical and chemical sensitization of SnO_2.[5] Recently, we have prepared the nanosized PdO-loaded SnO_2 nanoparticles through a reverse micelle method and revealed the chemical and the electrical sensitization effect of the PdO nanoparticles on the SnO_2 nanoparticles. In addition, the developed method was able to decrease the optimum amount of PdO because of its high dispersion on SnO_2 as compared with the conventional impregnation method.[21]

Received: May 25, 2012
Accepted: August 6, 2012
Published: August 7, 2012

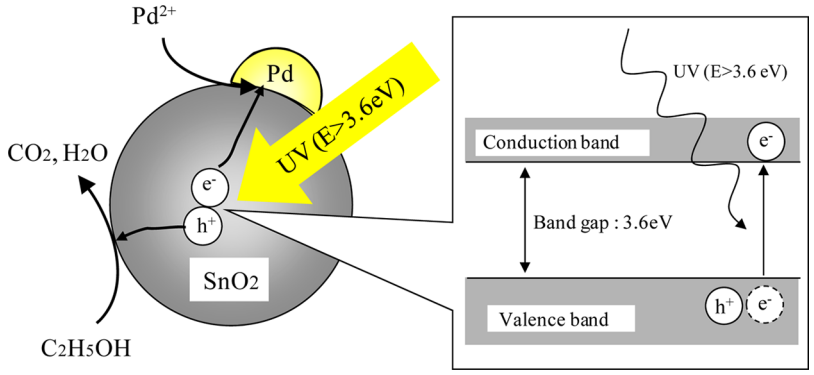

Figure 1. Schematic diagram of the deposition of Pd nanoparticles on the SnO_2 nanocrystal through a photochemical deposition.

As mentioned above, fundamental studies toward highly sensitive oxide semiconductor gas sensors have been carried out using a sol suspension of SnO_2 or receptor-loaded SnO_2 powder. However, a stable sol suspension of receptor-loaded SnO_2 nanocrystal has never been reported. If a stable sol suspension of receptor-loaded SnO_2 nanocrystal is obtained, it is possible to construct excellent gas sensing films that can satisfy the above three basic factors for improving the sensor response. Moreover, such stable sol suspensions of receptor-loaded SnO_2 nanocrystals are preferable for the fabrication of highly sensitive gas sensing films which can be integrated into a microgas sensor fabricated by a MEMS (micro electro-mechanical system) technique.[22,23] Therefore, preparation of a stable sol of receptor-loaded SnO_2 nanocrystal is a key for both the fundamental study and practical application of an oxide semiconductor gas sensor.

This study aimed to prepare a stable sol suspension of receptor-loaded SnO_2 nanocrystal. Pd was selected as the receptor. To fabricate a stable sol suspension of Pd-loaded SnO_2 nanocrystal, Pd nanoparticles were deposited on SnO_2 nanocrystals by an UV-assisted photochemical deposition.[24,25] In this method, ultraviolet (UV) light whose photon energy is larger than the band gap of SnO_2 (3.6 eV (= 344.1 nm)) was irradiated to the mixture of palladium chloride ($PdCl_2$), ethanol, and a suspension of SnO_2 nanocrystals (pH = 2). Then, photogenerated electrons (e^-) in the SnO_2 crystallite reduce palladium ions to Pd metal on the surface of SnO_2, as shown in Figure 1. Simultaneously, photogenerated holes (h^+) in the SnO_2 crystalline are consumed for the oxidation of ethanol to CO_2 and H_2O. The stable sol suspension of Pd-loaded SnO_2 nanocrystal obtained was used to fabricate thin-film type sensor devices (film thickness ~200 nm) via a spin-coating technique, and the electrical properties and the gas sensing properties of the thin-film type sensor devices were investigated.

EXPERIMENTAL SECTION

Preparation of Sol Suspensions of Pd-Loaded SnO_2 Nanocrystal. First of all, a stable sol suspension of SnO_2 nanocrystals was prepared through a hydrothermal treatment of stannic acid gel in an ammonium solution.[13,14] A volume of 100 mL of an aqueous solution of $SnCl_4 \cdot 5H_2O$ (1.0 mol/L) was hydrolyzed by dropping into 500 mL of an aqueous solution of NH_4HCO_3 (1.0 mol/L). The stannic acid gel obtained was washed by repeating the centrifuge (6000 rpm) and dispersion into the deionized water several times. Then, 15 g of the stannic acid gel was hydrothermally treated in 300 mL of an ammonia solution (pH = 10.5) under the pressure of 10 MPa at 200 °C for 3 h, and thus the sol suspension of SnO_2 nanocrystal was obtained. A hydrochloric acid, an aqueous solution of $PdCl_2$ (actually aqueous solution of $PdCl_4^{2-}$) and 1 mL of an ethanol were then added to 30 mL of the sol suspension of SnO_2 in a quartz beaker. Hydrochloric acid was added to adjust the pH of the suspension at pH 2 because $PdCl_4^{2-}$ ions precipitate as $Pd(OH)_2$ at a pH higher than 4.[26] The amount of Pd was controlled between 0.0625 to 1.0 mol % by controlling the additive amount of the aqueous solution of $PdCl_2$. Then UV light was irradiated on the suspension using a 250 W extra-high pressure mercury lamp (USH-250D, Ushio Inc.) for 10−120 min at room temperature under vigorous stirring. The gray-colored precipitate obtained was washed by repeating the centrifugation (10 000 rpm) and dispersion into deionized water two times in order to remove remaining chloride ion and ethanol. After the suspension was adjusted at pH 10.5 using the ammonium solution, stable sol suspensions of Pd-loaded SnO_2 nanocrystals were obtained. The morphology of the Pd-loaded SnO_2 nanocrystals was observed by means of transmission electron microscopy (TEM; JEM-2000EX, JEOL). The loading amount of Pd on the SnO_2 nanocrystal was analyzed by means of energy dispersive X-ray fluorescence analysis (XRF; EDX-800, Shimadzu Co. Ltd., X-ray source ; Rh K_α). The distribution of particle size and the electrophoretic mobility of Pd-loaded SnO_2 nanocrystal in the sol suspension were analyzed by means of a light scattering instrument with a He−Ne laser source (Photal ELS-8000, Otsuka Electronic Ltd.).

Sensor Fabrications and Gas Sensing Measurements. Sensor devices were fabricated on alumina substrates (9 mm × 13 mm × 0.38 mm) equipped with a pair of comb-type Au electrodes (electrode gap, 90 μm), as shown in Figure 2. Comb-type Au electrodes were fabricated on the alumina substrate by screen-printing using an Au paste (TR-1301, Tanaka Holdings Co., Ltd.), followed by calcination at 850 °C for 3 h in air. Then, a drop of the Pd-loaded SnO_2 suspension was spin-coated (spinning rate, 1500 rpm) on the alumina substrate with Au electrodes, followed by calcination at 430 °C for 3 h in air. The typical thickness of the fabricated sensing film was ~200 nm. The sensor devices obtained were put in a quartz tube and heated by a tube-type electric furnace. The sensor device was connected with a standard resistor in series, and the voltage across the standard

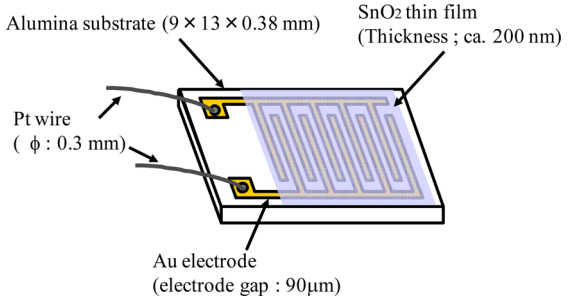

Figure 2. Structure of the thin-film type sensor device fabricated by spin-coating on the alumina substrate equipped with comb-type Au electrodes.

resistor was measured under an applied voltage of dc 4 V to evaluate the electrical resistance of the device. The electrical signal of the sensor devices was acquired with an electrometer (model 2701, Keithley Instruments Inc.). The electric resistances of the devices in air and in air containing target gas (200 ppm H_2) were measured. The sensor response (S = Rair/Rgas) was defined as the ratio of the electric resistance in air (Rair) to in target gas (Rgas).

RESULTS AND DISCUSSION

Characterization of Materials. The quantitative analysis of Pd on the SnO_2 nanocrystal was carried out by means of a XRF measurement. Samples for the XRF measurement were obtained by drying sol suspensions of Pd-loaded SnO_2 nanocrystals at 120 °C for 12 h. The peak ratio of Pd (K_α) to Sn (K_α) was measured, and the amount of Pd in each sample was determined by the calibration curve, which was obtained from the XRF measurement of reference samples. The reference samples were obtained by mixing the commercial PdO and SnO_2 powder. Figure 3 shows the dependence of the

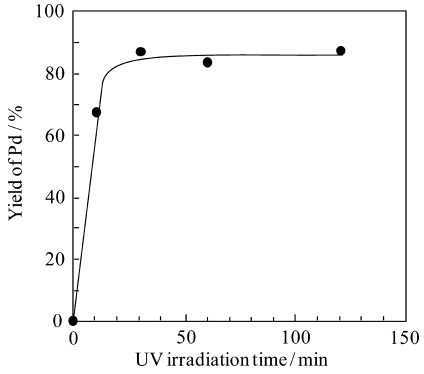

Figure 3. Dependence of yield of Pd on the irradiation time of UV light (0.5 mol % Pd-loaded SnO_2 nanocrystal).

yield of Pd on the UV light irradiation time for 0.5 mol % Pd-loaded SnO_2 nanocrystals. The yield of Pd was calculated from the ratio of the loaded amount of Pd calculated from the XRF measurement to the added amount of $PdCl_4^{2-}$. The yield of Pd was saturated at ~85% more than 30 min. This result indicates that the photochemical deposition of $PdCl_4^{2-}$ onto SnO_2 was completed in 30 min. Table 1 summarizes the dependence of

Table 1. Dependence of the Amount of Pd Deposited in the Samples on That of Pd Added (Irradiation Time of UV Light, 120 min)

added amount of Pd (mol %)	loaded amount of Pd (mol %)	yield (loading/added) (%)
0.0625	0.046	73.6
0.125	0.116	92.8
0.250	0.221	84.4
0.500	0.4385	87.7
1.000	0.852	85.2

the amount of Pd deposited on that of Pd added. In Table 1, the irradiation time of UV was set constant to 120 min at each sample. It was found that $PdCl_4^{2-}$ ions in the solution were not completely deposited on SnO_2 nanocrystals in all samples. As mentioned in the above discussion about the irradiation term of the UV-ray, the photochemical deposition of $PdCl_4^{2-}$ ions was saturated more than 30 min. Therefore, the reason for the difference between the amount of Pd particle on the SnO_2 nanocrystal and the added amount of $PdCl_4^{2-}$ ion is considered not to be the insufficiency of the UV irradiation term but other reasons. It seems that some of Pd particles deposited on the SnO_2 nanocrystals came unstuck from the surface of the SnO_2 during the centrifugation at 10 000 rpm for the removal of chloride ions and ethanol.

The dispersion state of Pd-loaded SnO_2 nanocrystals were characterized by means of light scattering measurement. Figures 4 and 5 show the appearance of samples and the particle size

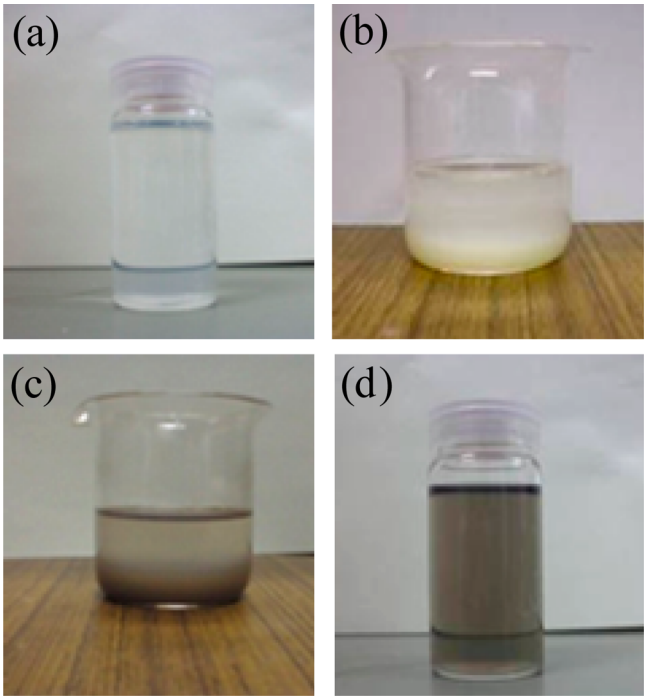

Figure 4. Photos of (a) as-prepared SnO_2 nanocrystal sol suspension, (b) a mixture of $PdCl_2$, ethanol, HCl and SnO_2 nanocrystal (pH 2), (c) Pd-loaded SnO_2 precipitate after UV irradiation, and (d) Pd-loaded SnO_2 nanocrystal sol suspension (pH 10.5).

distribution of as-prepared SnO_2 and Pd-loaded SnO_2, respectively. In Figure 5, the mean particle size and electrophoretic mobility of each sample are also represented. As shown in Figure 4a, the as-prepared SnO_2 sol was transparent because SnO_2 nanocrystals are dispersed stably in an ammonia solution. The size distribution of SnO_2 nanocrystals were monodispersed, with mean particle size of 5.7 nm and electrophoretic mobility of -3.10×10^{-4} cm^2/V s. However, after the aqueous solution of $PdCl_4^{2-}$, the hydrochloric acid and ethanol were added to the as-prepared SnO_2 sol (pH = 2) and the SnO_2 nanocrystals were agglomerated and sedimented immediately as shown in Figure 4b, because pH 2 is close to the isoelectric point of the SnO_2 particles.[27] After the photochemical deposition of the Pd particles, the color of the suspension changed from white to gray as shown in Figure 4c. The change in color clearly indicates that Pd particles were precipitated on the SnO_2 nanocrystals. The gray colored cloudy suspension became a clear stable when the solution pH was adjusted to 10.5 using an ammonia solution as shown in Figure 4d. This is because the negative charge of the SnO_2 surface was recovered by adjusting the pH of solution to 10.5. As shown in Figure 5b, the mean particle size and absolute value of electrophoretic mobility were increased and decreased, respectively, by the deposition of Pd. These finding suggest

dx.doi.org/10.1021/am300941a | ACS Appl. Mater. Interfaces 2012, 4, 4231−4236

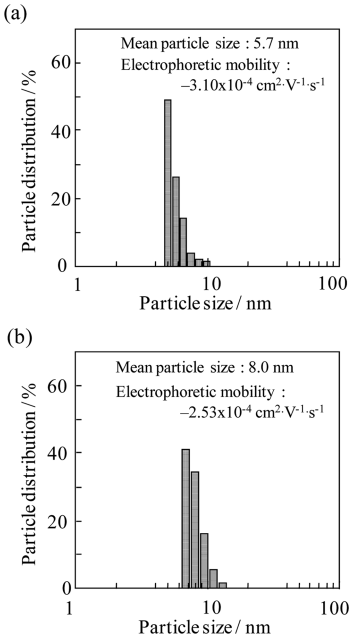

Figure 5. Particle size distributions and electrophoretic mobility of (a) a sol suspension of SnO_2 nanocrystal and (b) 0.5 mol % Pd-loaded SnO_2 nanocrystal.

that the Pd deposition changed the surface state of SnO_2. In a basic aqueous solution, the surface −OH groups of oxide interact with the surrounding water molecules as follows:[27,28]

$$-SOH + H_2O \Leftrightarrow -SO^- + H_3O^+ \quad (S: \text{surface of oxides}) \tag{1}$$

This makes the surface of SnO_2 particles negative. In contrast, for the surface of neat metal, the interaction is weaker, as compared with oxides such as SnO_2. Therefore, the negative charge density of the Pd-loaded SnO_2 surface is smaller than that of the as-prepared SnO_2 surface, leading to a decrease in the absolute value of the electrophoretic mobility.

The morphology of the Pd-loaded SnO_2 nanocrystals was observed by means of a TEM. Samples for the TEM observation were obtained by deposition of the Pd-loaded SnO_2 sol on a carbon-supported Cu mesh grid. Figure 6 shows TEM images of Pd-loaded SnO_2 nanocrystals with different Pd loading amounts. In both samples, SnO_2 particles were elliptical in shape, ∼4 nm in width, and ∼10 nm in length. However, the size and shape of Pd on the SnO_2 crystals was different depending on the loading amount of Pd. For 0.5 mol % Pd addition, the Pd particles on SnO_2 nanocrystals were spherical having ∼3 nm diameter. On the other hand, for 1.0 mol % Pd addition, Pd particles grown to be an elliptical shape of ∼4 nm in width and ∼10 nm in length. Moreover, the tip of elliptical-shaped Pd particles seem to be in contact with SnO_2 particles. This result indicates that $PdCl_4^{2-}$ ions were reduced on predeposited spherical Pd particles one after another. Figure 7 shows the energy diagram of the photochemical deposition system for the Pd and SnO_2 at pH 2. In this figure, the conduction band edge of SnO_2 (E_{CB}), valence band of SnO_2 (E_{VB}), work function of Pd, and the reduction potential of $PdCl_4^{2-}$ to Pd^0 were calculated using the values as reported elsewhere.[29−33] As shown in Figure 7, Pd has a larger work function as compared with SnO_2. Therefore, electrons generated by the excitation light from the valence band to the conduction band of SnO_2 can preferentially spill into the

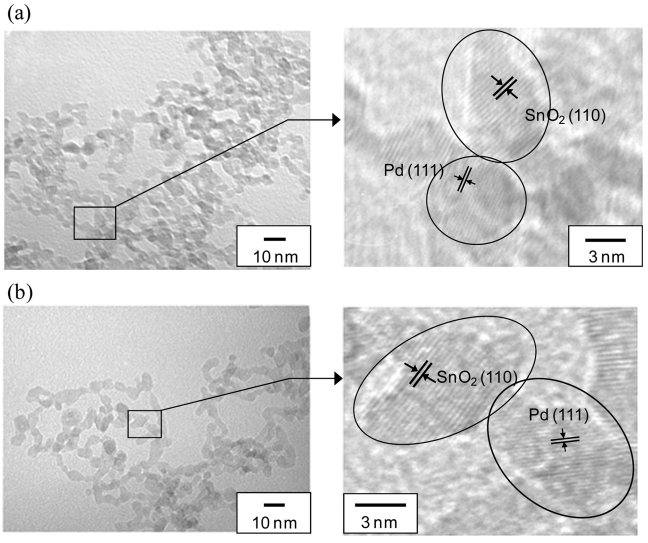

Figure 6. TEM images of Pd-loaded SnO_2 nanocrystal: (a) 0.5 mol % and (b) 1.0 mol %.

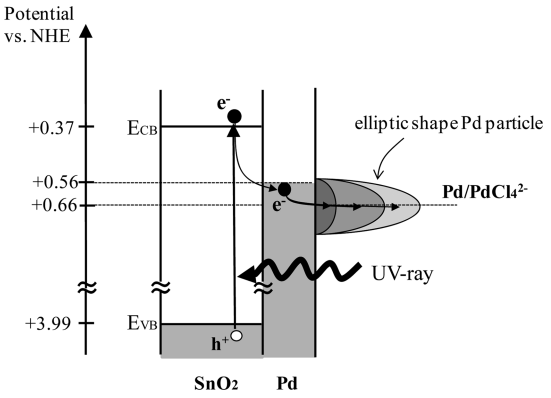

Figure 7. Energy diagram of the photochemical deposition system for the Pd and SnO_2 (pH 2).

predeposited Pd^0 atom, followed by reducing the $PdCl_4^{2-}$ to Pd onto predeposited Pd^0 atoms one and another. Thus, photochemical deposited $PdCl_4^{2-}$ ions form Pd particles of an elliptical shape on SnO_2 nanocrystals.

Sensor Properties. It has been reported that loading of Pd (or PdO) on SnO_2 promotes the gas sensitivity to inflammable gases and that this originates from both the electrical and chemical sensitization effects.[5,21] In the electrical sensitization, PdO acts as an acceptor of electrons, so that electrons are removed from the SnO_2 surface to PdO. This causes a drastic increase in the electrical resistance. Such an increase in the electrical resistance promotes changes in the electrical resistance between air and inflammable gases. Thus, the electric resistance measurement in an air atmosphere is effective to check whether the deposited Pd on SnO_2 has a electrical sensitization effect or not. Figure 8 shows the dependence of electric resistances on the loading amount of Pd for two thin film-type sensor devices using Pd-loaded SnO_2 nanocrystals and as-prepared SnO_2 nanocrystals, respectively. In the range of the measurement temperature (250−400 °C), Pd on the SnO_2 nanocrystals is considered to be oxidized to PdO in air according to the calculation from thermodynamic data.[34] As shown in Figure 8a,b, in all samples using Pd-loaded SnO_2 nanocrystals, the electric resistance of sensing films was larger

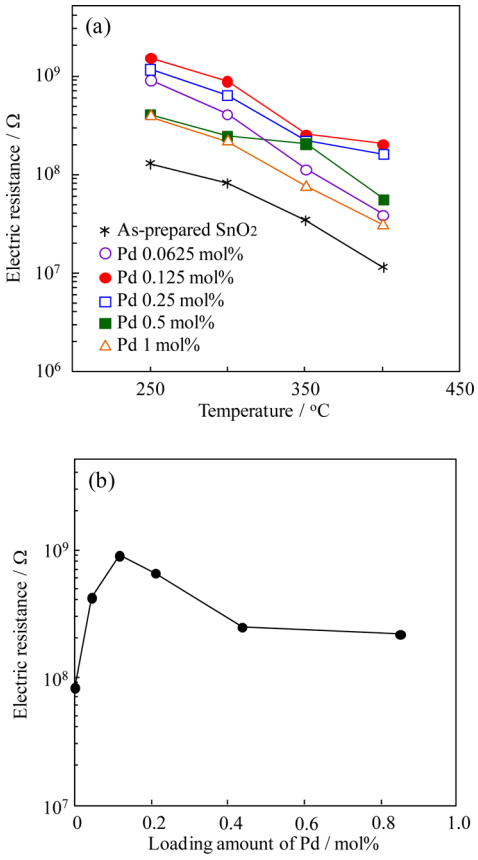

Figure 8. Dependence of electrical resistance for the thin-film type sensor elements on (a) the operating temperature and (b) on the loading amount of Pd at 300 °C.

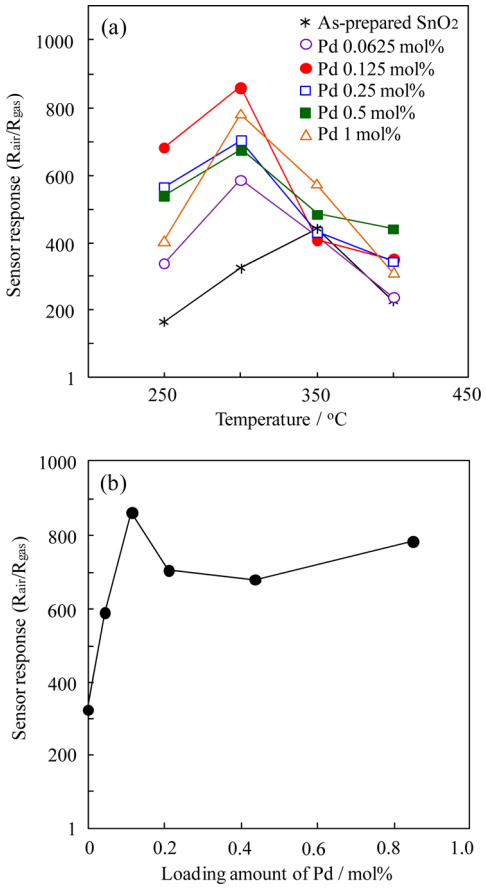

Figure 9. Dependence of the sensor response to 200 ppm H_2 for thin-film type sensor elements on (a) the operating temperature and (b) the loading amount of Pd for the thin film-type sensor device at 300 °C.

than that for as-prepared SnO_2 nanocrystals. This result indicates that Pd (actually PdO) on the SnO_2 nanocrystals demonstrated the electrical sensitization effect. The maximum of the increase in the electrical resistance was obtained at 0.125 mol % Pd loading. On the other hand, further loading of Pd rather decreased the electrical resistance, as shown in Figure 8b. This tendency is consistent with our previous report about a thick-film type sensor device fabricated by a reverse micelle method.[21] As mentioned in the above discussion about TEM observation, the increase in the loading amount of Pd increased the particle size of Pd rather than the number of Pd on SnO_2 nanocrystals. Therefore, the increase in the particle size might hinder the electron transfer from SnO_2 to PdO but promote that from metallic Pd to PdO, decreasing the electrical resistance. The detail of the mechanism is currently under consideration.

Figure 9 shows the dependence of the sensor response to 200 ppm H_2 on the loading amount of Pd for thin film-type sensor devices using Pd-loaded SnO_2 nanocrystals and as-prepared SnO_2 nanocrystals. The maximum sensor response was obtained at 0.125 mol %. This tendency well correlates with the dependence of electrical resistance on the loading amount of Pd as shown in Figure 8b. Therefore, it can be said that the electrical interaction of Pd and SnO_2 is the one of the main causes of the sensitivity promotion. Another remarkable point brought about by the Pd deposition is that the temperature, in which the maximum sensor response was observed, was decreased, as shown in Figure 9a. It has been reported that palladium on SnO_2 promotes the catalytic combustion of reducing gases such as CO, H_2, and C_3H_8 (chemical sensitization).[5,15] Thus, Pd particles deposited via photochemical deposition activated the catalytic combustion of H_2 at lower temperatures, leading to a decrease in the operating temperatures.

CONCLUSIONS

A stable sol suspension of Pd-loaded SnO_2 nanocrystals, which is valid for both fundamental studies of semiconductor gas sensors and fabrications of micro gas sensors, was prepared in order to investigate the gas sensing properties of thin-film type sensor devices using Pd-loaded SnO_2 nanocrystals. Pd nanoparticles were loaded on SnO_2 nanocrystals through a photochemical deposition of $PdCl_4^{2-}$ under UV irradiation. The Pd-loaded SnO_2 nanocrystals obtained were subjected to the fabrication of thin-film type sensor devices using a spin-coating technique, and their sensor responses to H_2 were measured. Pd was successfully loaded onto SnO_2 nanocrystals (5.7 nm) by the photochemical deposition of $PdCl_4^{2-}$. It was found that the Pd nanoparticles deposited tended to grow to an elliptical shape because electron generated by UV-irradiation can spill into predeposited Pd. Owing to the successful synthesis of Pd-loaded SnO_2 nanocrystals, a significantly high sensor response to H_2 (exceeding 900) was obtained. The maximum sensor response to H_2 was obtained at a very small amount of Pd loading (0.125 mol %) due to the realization of high dispersion of Pd on SnO_2 nanocrystals. Moreover, the

dx.doi.org/10.1021/am300941a | ACS Appl. Mater. Interfaces 2012, 4, 4231−4236

present Pd loading successfully lowered the operating temperature of the devices. Our developed Pd-loaded SnO_2 nanocrystals demonstrated the feasibility of high-performance gas sensors having super high sensitivity and operative at lower temperatures.

AUTHOR INFORMATION

Corresponding Author

*E-mail: yuasa@mm.kyushu-u.ac.jp.

Notes

The authors declare no competing financial interest.

ACKNOWLEDGMENTS

This work has been financially supported by a Nippon Sheet Glass Foundation for Materials Science and Engineering.

REFERENCES

(1) Ihokura, K.; Watson, J. *The Stannic Oxide Gas Sensor: Principles and Applications*; CRC Press: Boca Raton, FL, 1994.
(2) Göpel, W.; Schierbaum, K. D. *Sens. Actuators, B* **1995**, *26*−*27*, 1−12.
(3) Yamazoe, N.; Sakai, G.; Shimanoe, K. *Catal. Surv. Asia* **2003**, *7*, 63−75.
(4) Yamazoe, N.; Fuchigami, J.; Kishikawa, M.; Seiyama, T. *Surf. Sci.* **1972**, *86*, 335−344.
(5) Yamazoe, N. *Sens. Actuators, B* **1991**, *5*, 7−19.
(6) Xu, C.; Tamaki, J.; Miura, N.; Yamazoe, N. *Sens. Actuators, B* **1991**, *3*, 147−155.
(7) Yamazoe, N.; Shimanoe, K. *J. Electrochem. Soc.* **2008**, *155*, J85−J92.
(8) Yamazoe, N.; Shimanoe, K. *J. Electrochem. Soc.* **2008**, *155*, J93−J98.
(9) Yamazoe, N.; Shimanoe, K. *Sens. Actuators, B* **2011**, *160*, 1352−1362.
(10) Shimizu, Y.; Maekawa, T.; Nakamura, Y.; Egashira, M. *Sens. Actuators, B* **1998**, *46*, 163−168.
(11) Sakai, G.; Matsunaga, N.; Shimanoe, K.; Yamazoe, N. *Sens. Actuators, B* **2001**, *80*, 125−131.
(12) Matsunaga, N.; Sakai, G.; Shimanoe, K.; Yamazoe, N. *Sens. Actuators, B* **2003**, *96*, 226−233.
(13) Baik, N. S.; Sakai, G.; Miura, N.; Yamazoe, N. *Sens. Actuators, B* **2000**, *63*, 74−79.
(14) Sakai, G.; Baik, N. S.; Miura, N.; Yamazoe, N. *Sens. Actuators, B* **2001**, *77*, 116−121.
(15) Yamazoe, N.; Kurokawa, Y.; Seiyama, T. *Sens. Actuators* **1983**, *4*, 283−289.
(16) Maekawa, T.; Tamaki, J.; Miura, N.; Yamazoe, N. *Chem. Lett.* **1991**, *20*, 575−578.
(17) Lantto, V.; Mizsei, J. *Sens. Actuators, B* **1991**, *5*, 21−25.
(18) Maekawa, T.; Tamaki, J.; Miura, N.; Yamazoe, N. *Sens. Actuators, B* **1992**, *9*, 63−69.
(19) Schierbaum, K. D.; Geiger, J.; Weimar, U.; Göpel, W. *Sens. Actuators, B* **1993**, *13*−*14*, 143−147.
(20) Khodadadi, A.; Mohajerzadeh, S. S.; Mortazavi, Y.; Miri, A. M. *Sens. Actuators, B* **2011**, *80*, 267−271.
(21) Yuasa, M.; Masaki, T.; Kida, T.; Shimanoe, K.; Yamazoe, N. *Sens. Actuators, B* **2009**, *136*, 99−104.
(22) Benkstein, K. D.; Martinez, C. J.; Li, G.; Meier, D. C.; Montgomery, C. B.; Semanncik, S. *J. Nanopart. Res.* **2006**, *8*, 809−822.
(23) Benkstein, K. D.; Semancik, S. *Sens. Actuators, B* **2006**, *113*, 445−453.
(24) Zhang, F.; Chen, J.; Zhang, X.; Gao, W.; Jin, R.; Guan, N. *Catal. Today* **2004**, *93*−*95*, 645−650.
(25) Chien, S. H.; Liou, Y. C.; Kuo, M. C. *Synth. Met.* **2005**, *152*, 333−336.
(26) Pourbaix, M. *Atlas of Electrochemical Equilibria in Aqueous Solutions*; Pergamon Press: Oxford, U.K., 1966.
(27) Pereira, G. J.; Castro, R. H. R.; Hidalgo, P.; Gouvêa, D. *Appl. Surf. Sci.* **2002**, *195*, 277−283.
(28) Zuyi, T.; Wenming, D. *J. Colloid Interface Sci.* **1998**, *208*, 248−251.
(29) Tada, H.; Hattori, A.; Tokihisa, Y.; Imai, K.; Tohge, N.; Ito, S. *J. Phys. Chem. B* **2000**, *104*, 4584−4587.
(30) Taghizadeh, A.; Lawrence, M. F.; Miller, L.; Anderson, M. A.; Serpone, N. *J. Photochem. Photobiol., A* **2000**, *130*, 145−156.
(31) Michaelson, H. B. *J. Appl. Phys.* **1977**, *48*, 4729−4733.
(32) Trasatti, S. *Pure Appl. Chem.* **1986**, *58*, 955−966.
(33) Jacobs, J. W. M. *J. Phys. Chem.* **1986**, *90*, 6507−6517.
(34) Mallika, C.; Sreedharan, O. M.; Gnanamoorthy, J. B. *J. Less-Common Met.* **1983**, *95*, 213−220.